Simulation of fluid flow and gaseous radiation heat transfer in a natural gas-fired furnace

Ge Song, Tor Bjørge, Jens Holen and Bjørn F. Magnussen
Department of Applied Mechanics, Thermo- and Fluid Dynamics, The Norwegian Institute of Technology, Trondheim, Norway

Introduction

Thermal radiation heat transfer involving gases is usually an important mode of heat transfer (even under non-sooting conditions) in high-temperature furnaces, such as boilers and industrial furnaces. In the combustion of hydrocarbon fuels, the familiar products of combustion – H_2O, CO_2, CO – are particularly important owing to their comparatively high absorptivities and emissivities in the near infrared region. Real combustion gases are non-gray; therefore, the spectral variation of the radiative properties must be accounted for in the solution for accurate prediction of radiation heat transfer. In earlier studies, the emitting gaseous medium was divided into statistically independent homogeneous and isothermal columns. The gray gas, isothermal assumption can lead to considerable errors in large-scale fires[1]. Other works use non-gray band models[2,3] which relax the gray gas, isothermal assumption. Taine[4] and Hartmann *et al.*[5] carried out line-by-line calculations for single absorption bands of CO_2 and H_2O respectively. The line-by-line results are used to check their tabulated data for statistical narrow-band parameters. In a more recent paper[6], high-resolution spectral correlations are considered in order to analyse the fluctuation of radiative intensity at some specified wavelengths. The purpose of this paper is to investigate the spectral characteristic of combustion gases and illustrate that the gas radiation properties vary considerably with wavelength. The Goody statistical narrow-band model[7] with exponential-tailed inverse line-strength distribution and the Curtis-Godson approximation are used to calculate the real gas radiative properties in this work. An investigation of the spectral characteristics of two bands for CO_2 and four bands for H_2O is described by generalized expressions for computing the band parameters $(\overline{S/d})$ and $(\overline{\gamma/d})$.

Theoretical analysis

General transport equation

The partial differential equations which describe the conservation of mass species, momentum and heat in conjunction with turbulence models, can be expressed in a generalized form as

International Journal of Numerical Methods for Heat & Fluid Flow
Vol. 7 No. 2/3, 1997, pp. 169-180.

$$\frac{\partial}{\partial t}(\rho\Phi) + \frac{\partial}{\partial x_i}(\rho u_i \Phi) = \frac{\partial}{\partial x_i}(\Gamma_{eff}\frac{\partial \Phi}{\partial x_i}) + S_\Phi \quad (1)$$

where Φ is a set of n variables and Γ_{eff} is the transport coefficient of the variable Φ. S_Φ is called the source term. Values for different Φ, Γ_{eff} and S_Φ are listed in Table I.

Conserved property	Φ	Γ_{eff}	S_Φ
Overall mass	1	0	0
Species mass fraction	m_{fu}	μ_{eff} / σ_{fu}	R_{fu} [8]
Momentum	u_k	μ_{eff}	$\frac{\partial}{\partial x_i}[-p\delta_{ik} + \mu_{eff}(\frac{\partial u_i}{\partial x_k} + \frac{\partial u_k}{\partial x_i} - \frac{2}{3}\delta_{ik}\frac{\partial u_l}{\partial x_l})] + B_k$
Turbulent kinetic energy	k	μ_{eff} / σ_k	$G - \rho\varepsilon$
Dissipation rate	ε	$\mu_{eff} / \sigma_\varepsilon$	$C_1 \frac{\varepsilon}{k} G - C_2 \rho \frac{\varepsilon^2}{k}$
Enthalpy	h	k / C_p	$R_{rad} + G + \frac{Dp}{Dt}$
G is called the turbulent production $G = \mu_t(\frac{\partial u_i}{\partial x_k} + \frac{\partial u_k}{\partial x_i} - \frac{2}{3}\frac{\partial u_l}{\partial x_l}\delta_{ik})\frac{\partial u_i}{\partial x_k}$			

Table I.
Variables in the general transport equation

C_μ	C_1	C_2	σ_k	σ_ε	σ_{fu}	σ_h
0.09	1.44	1.92	1.0	1.30	0.9	0.9

The three-dimensional turbulent or laminar flow, heat and mass transfer simulation has been performed with the computer code KAMELEON developed at the Division of Applied Mechanics, Thermo- and Fluid Dynamics, The Norwegian Institute of Technology. The code, which uses a control volume based on finite difference technique, solves the conservation equations (including an appropriate form of the Navior-Stokes equation) and the pressure is solved by the SIMPLE algorithm of Patankar[8]. This gives a set of discretized equations which are solved by TDMA (Tri-diagonal-matrix-algorithm) giving the values of the velocity components, pressure and temperature, etc. in each cell. A staggered grid is used to obtain a consistent connection between the pressure gradient and the velocity field. The velocities are calculated at the boundaries of the control volumes of the original grid.

Narrow-band statistical model

Much progress has been done in the understanding of molecular gas radiation during the last few decades; in particular, the radiation from water vapour and

carbon dioxide, which is of great importance in the combustion of hydrocarbon fuels. The radiative properties of a gas vary strongly and rapidly with wavelength, and the wavelength dependence of these properties causes additional complication. Consequently, the variation of the radiative properties with the electromagnetic spectrum must be accounted for. In modelling the spectral behaviour of combustion gases, an important feature of these studies is related to the accuracy of the (narrow) band statistical model for describing the absorptivity of H_2O and CO_2. The narrow band model, which uses the characteristics of the individual line shapes, widths and *spacings* to derive band characteristics within a defined wavelength or frequency interval, is employed here.

Approximations for the transmissivity τ_ν at a wave-number ν is given by Goody[9], using the two-parameter exponential-tailed distribution with the Curtis-Godson approximation for inhomogeneous gas paths,

$$\tau_\nu = exp\left[-2\left(\frac{\gamma}{d}\right)_\nu\left(\sqrt{1+\frac{\left(\frac{S}{d}\right)_\nu \cdot u_i}{\left(\frac{\gamma}{d}\right)_\nu}}-1\right)\right] \tag{2}$$

where $(\overline{S/d})_\nu$ is the mean line-intensity to spacing ratio and $(\overline{\gamma/d})_\nu$ is the mean line-width to spacing ratio. u_i is expressed as follows,

$$u_i = P_i\frac{T}{273}l \tag{3}$$

where P_i is the partial pressure of the ith species in atm, and l is the physical path length. The shape of spectral lines is an intrinsic property of radiating gases influencing the absorption and emission characteristics. The program uses the data of Ludwig *et al.*[10] and the models of Grosshandler[11] to determine the two parameters $(\overline{S/d})$ and $(\overline{\gamma/d})$.

Spectral radiation intensity

Consider a volume of high temperature absorbing/emitting (but no scattering) gas, with non-uniform temperature concentration, and non-reflecting, cool boundaries. The intensity of radiation within such an enclosure along the path length s is attenuated by absorption and enhanced by emission,

$$\frac{dI_\nu}{ds} = \alpha_\nu(I_{B\nu} - I_\nu) \tag{4}$$

This equation describes the changes in intensity along a path length ds at a wave-number ν. The first term on the right side of equation(4) represents the contributions to the intensity by emission from the elemental volume of the medium. The second term is the extinction of radiant energy owing to absorption. α_ν is the absorption coefficient at a wave-number ν. $I_{B\nu}$ is the black-body intensity at a wave-number ν,

$$I_{B\nu} = \frac{2C_1\nu^3}{exp(C_2\nu/T) - 1} \tag{5}$$

The radiation constants are $C_1 = 0.5955 \times 10^8$ and $C_2 = 14{,}387.69$ μmK. The optical depth κ_ν is defined as,

$$\kappa_\nu(s) \equiv \int_0^s \alpha_\nu ds \tag{6}$$

Multiplying through by $e^{k\nu(s)}$ on both sides of equation (4) gives,

$$e^{\kappa_\nu(s)} \cdot \frac{dI_\nu}{d\kappa_\nu(s)} + I_\nu \cdot e^{\kappa_\nu(s)} = \frac{d}{d\kappa_\nu(s)}[I_\nu \cdot e^{\kappa_\nu(s)}] = I_{B\nu} \cdot e^{\kappa_\nu(s)} \tag{7}$$

Integrating over the optical depth $\kappa_\nu(s)$ from $s = 0$ to s, we get the integrated form of radiation transfer equation described by [12],

$$I_\nu(s) = I_\nu(0)exp[-\int_0^s \kappa_\nu(s')ds'] + \int_0^s I_{B\nu}(s')exp[-\int_s^{s'} \kappa_\nu(s'')ds'']\kappa_\nu(s')ds' \tag{8}$$

The physical interpretation of equation (8) is quite evident. The first term in equation (8) on the right hand side, $I_\nu(0)exp[-\int_0^s k_\nu(s')ds']$, denotes energy that originated from the entrance of the column at temperature T and that has been attenuated as a result of absorption by the factor $exp[-\int_0^s k_\nu(s')ds']$. The second term in equation (8) represents augmentation of the intensity at s', resulting from energy emission from all of the elemental volumes, reduced by exponential attenuation between each point of emission s'' and the location s'.

The major complexity of equation (8) is associated with the functional form of the absorption coefficient, $k_\nu(s)$, which varies in a complex manner with the chemical species, wave-number, temperature and pressure. The numerical form of equation (8) is,

$$I_\nu(y) = I_\nu(b) * \tau_{\nu,\overline{b;y}} + \sum_{i=1}^{M} I_{B\nu}(\tau_{\nu,\overline{i-1;y}} - \tau_{\nu,\overline{i;y}}) \tag{9}$$

where $\tau_\nu = \exp(-\int_0^s k_\nu d(s'))$ is called transmittance along a non-homogeneous path between 0 and s. The index b stands for background radiation along the pathline. M is the total number of intervals across the furnace. This assumes no influence of radiation coming from other directions on the intensity along the path.

Furnace consideration

A typical side-port fired regenerative glass melting furnace is shown in Figure 1. In regenerative furnaces, both the burner port and the exhaust port are located along the sides of the furnace, which are cyclically fired. The number of burners per side can differ from furnace to furnace ranging from three to 15. Each port contains two burners, consisting of the injection of both fuel and the primary air into a stream of the preheated secondary air. The regenerators are used to heat

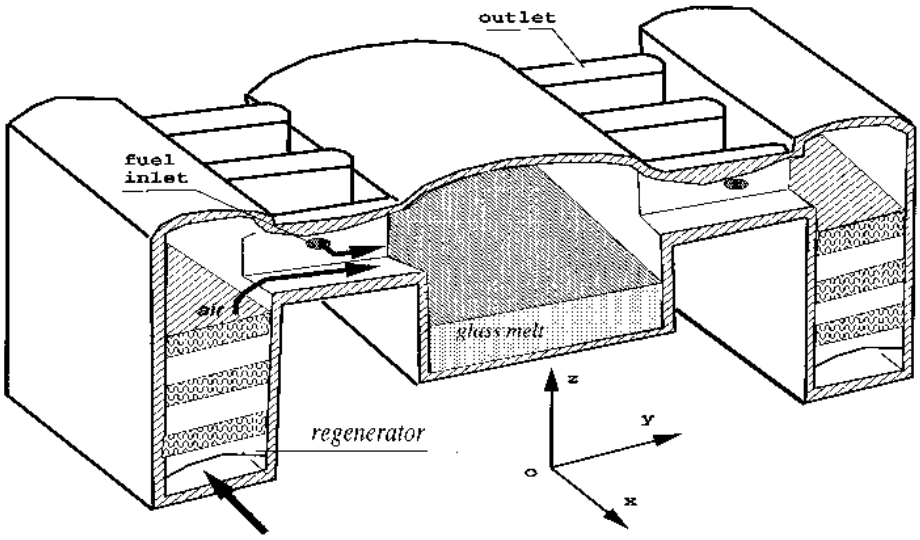

Figure 1.
Side-port fired regenerative glass melting furnace

the combustion air. The fuel and air are mixed in the burner port before entering the chamber.

The mass flow rate of fuel and primary air is 7.09kg/s and the fuel and air are injected at ambient temperature. The secondary air is preheated to 1,200K. The velocity at the secondary air inlet is 6.25m/s. Because of symmetry, only the processes in half a burner system compartment have been simulated in the present study. In the computational calculation, we have analysed a $9.9 \times 13.25 \times 2.4 m^3$ furnace using a grid with $13 \times 26 \times 15$ nodes in X-, Y- and Z-directions respectively (see Figure 2). The black walls are at a constant temperature T_w = 423K.

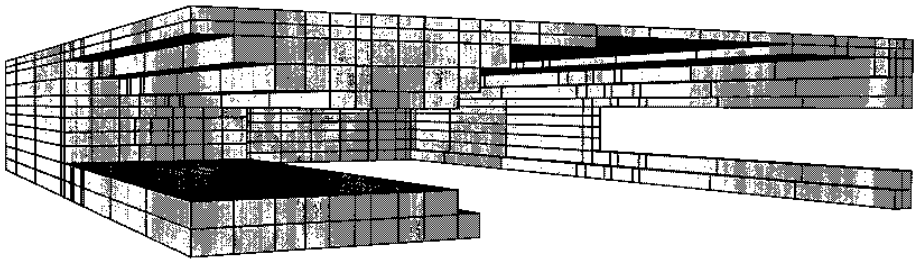

Figure 2.
Half of the combustion chamber

Results and discussion

The numerical study is based on a three-directional simulation of the fluid flow, mass and heat transfer inside the furnace.

Figure 3 shows the predicted temperature distribution in a plane perpendicular to the bottom of the furnace (Y-Z plane). The flow pattern, presented by arrows, is mainly a jet crossing the furnace from the inlet to the outlet port.

Figure 4 depicts temperature iso-contours and velocity vectors in a horizontal plane at Z = 1.133m. Figure 4 contains the inlet and the outlet port. It is clearly shown that the injection jet is deflected by the secondary air flow. The temperature reaches its highest value of 2,668.8K in the reaction region in Figure 4, because the horizontal plane of Z = 1.133m is at the height as the injected flows. The high specified temperature of the secondary air also increases the temperature level.

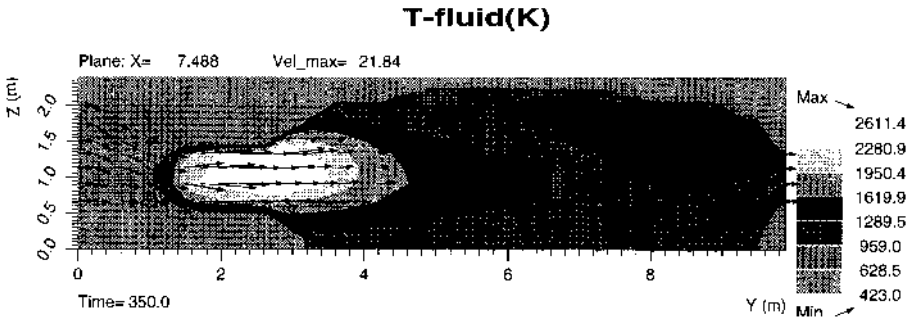

Figure 3.
Temperature (K) and velocity vectors shown in a plane normal to the X-axis (X = 7.488m)

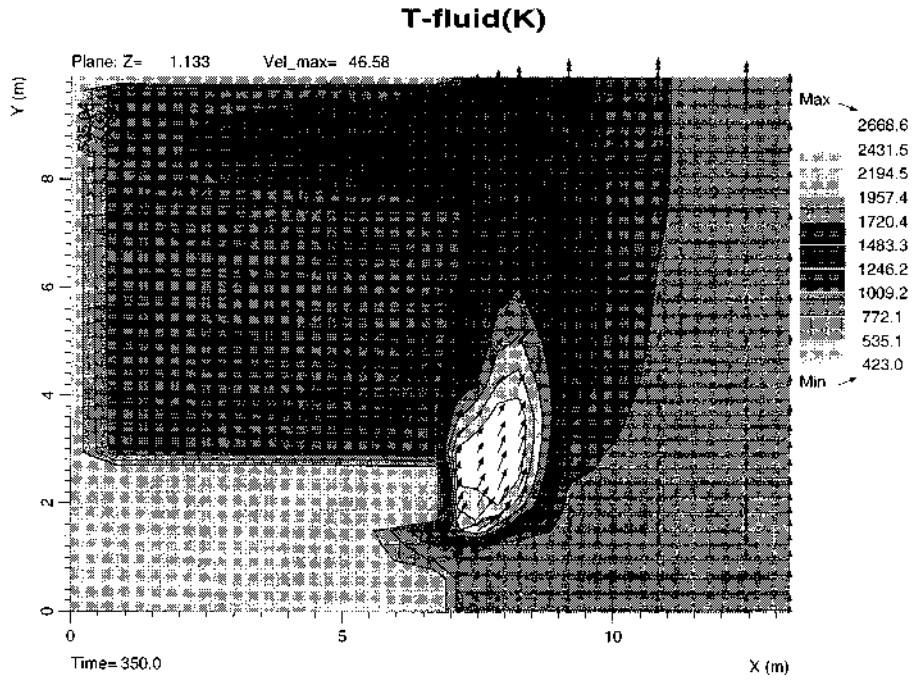

Figure 4.
Temperature (K) and velocity vectors shown in a plane normal to the Z-axis (Z = 1.133m)

Figure 5 shows the profile of the axial velocity component V(m/s) and vectors in longitudinal vertical planes at X = 7.874m. Because of the upper recirculation zone near the roof and the poor oxygen content region near the outlet, a small amount of unburned fuel appears. This can be improved by changing the

inclination of the burner. The iso-contours of both the transverse and axial velocity profiles as well as their vectors are displayed in Figure 6. Both the deflection of the fuel jet and the recirculation zone can be clearly observed.

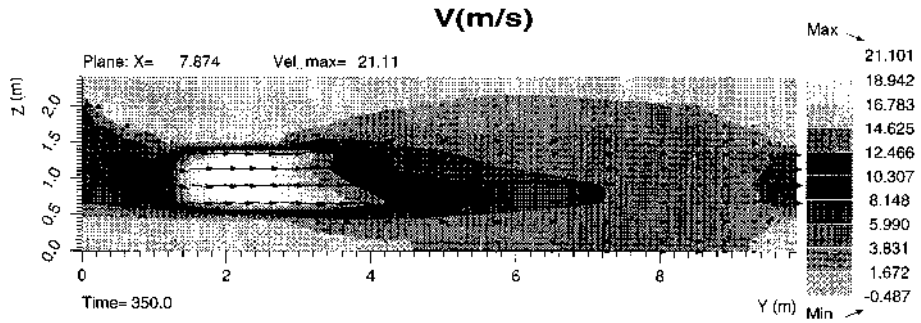

Figure 5. Axial velocity component V(m/s) and vectors shown in a plane normal to the X-axis (X = 7.874m)

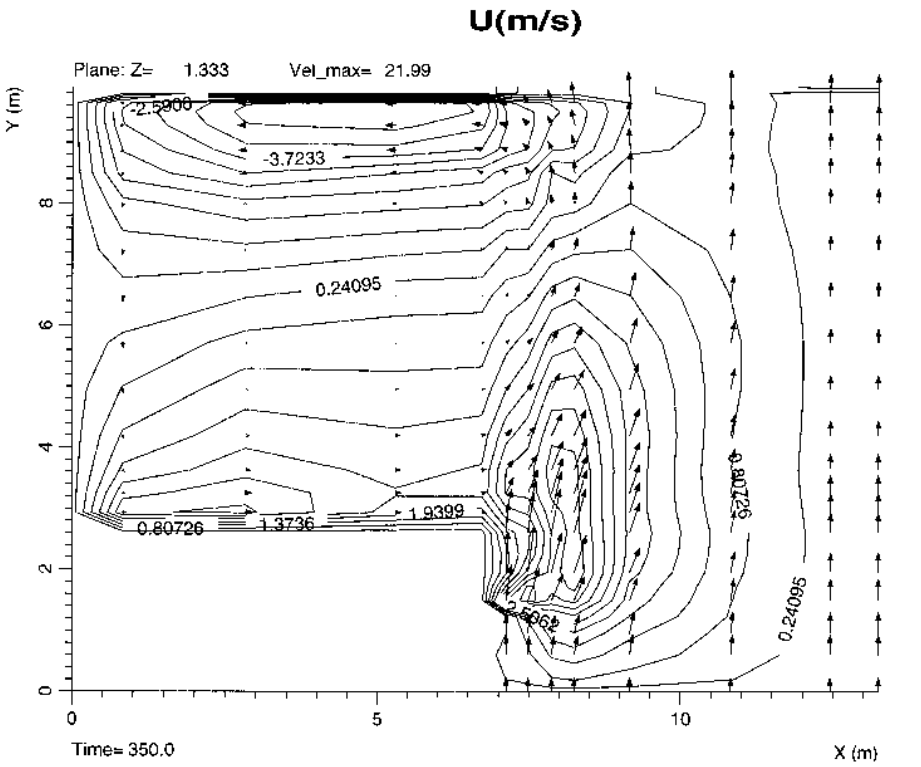

Figure 6(a). Tansverse velocity component (m/s) and vectors shown in a plane normal to the Z-axis (Z = 1.333m)

The profiles of turbulent kinetic energy are plotted in a side-viewed plane in Figure 7. The k distributions show high turbulent kinetic energies near the centre and lower values around the edges.

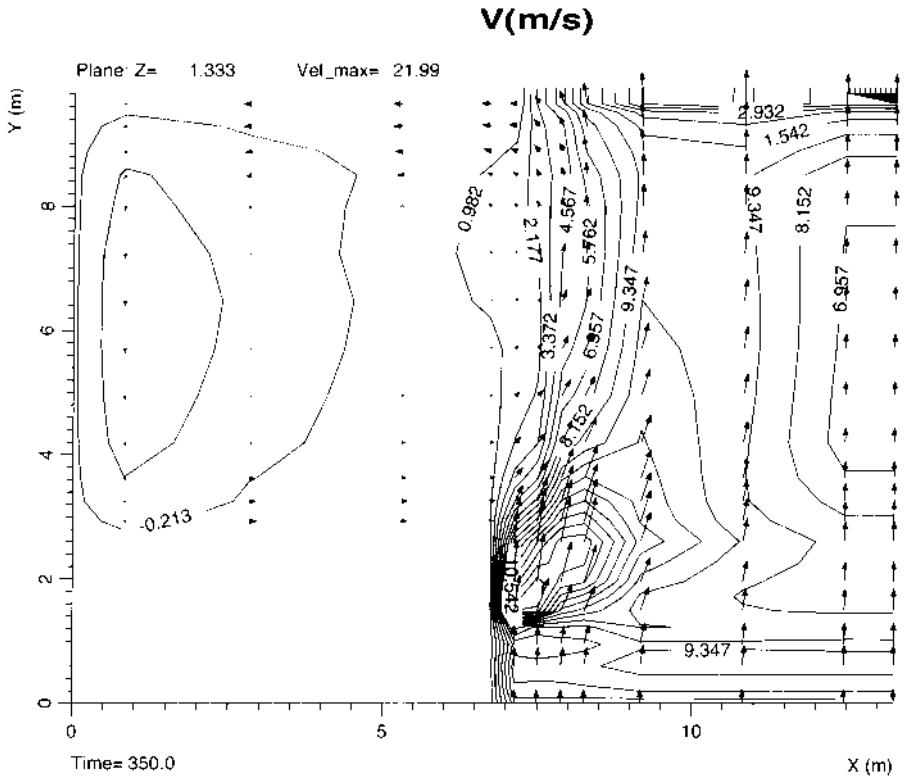

Figure 6(b).
Axial velocity component (m/s) and vectors shown in a plane normal to the Z-axis (Z = 1.333m)

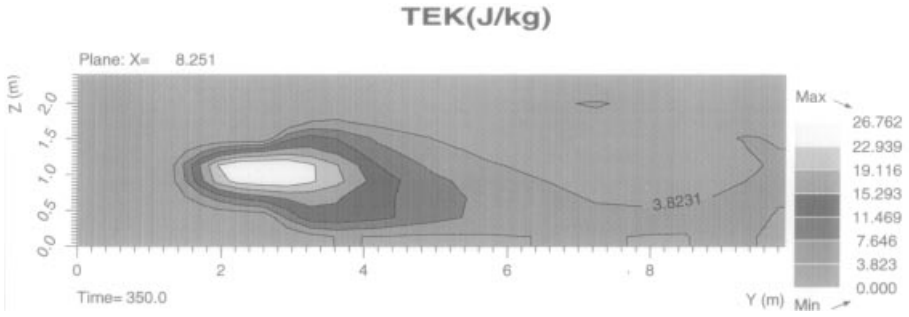

Figure 7.
Turbulent kinetic energy k (J/kg) in a plane normal to the X-axis (X = 8.251m)

In Figure 8, the average absorptivity α, determined from a narrow-band model, is compared with a result based on a line-by-line calculation[4]. A reasonable agreement is obtained.

The prediction of mass fraction (CO_2 + H_2O) and temperature profiles along the Y-axis at X = 7.13m and Z = 0.91m are shown in Figures 9(a) and 9(b) respectively. Two different grids are used in order to assess the grid dependence of the simulations. The agreement between the results using the coarse grid (13 $\times$ 26 $\times$ 15) and the fine grid (27 $\times$ 39 $\times$ 18) is good. The similar shapes of these

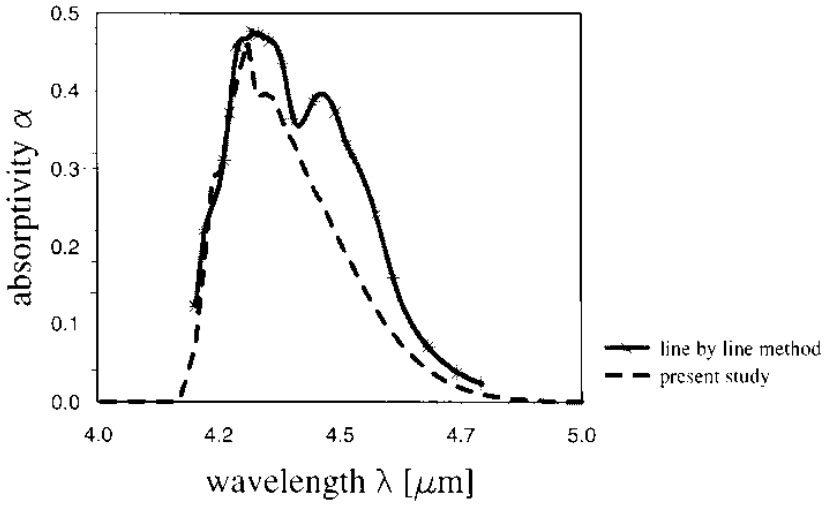

Figure 8.
The spectrum of the 4.3μm band CO_2 for L = 2cm, T = 2,900K and Y_{CO_2} = 0.25

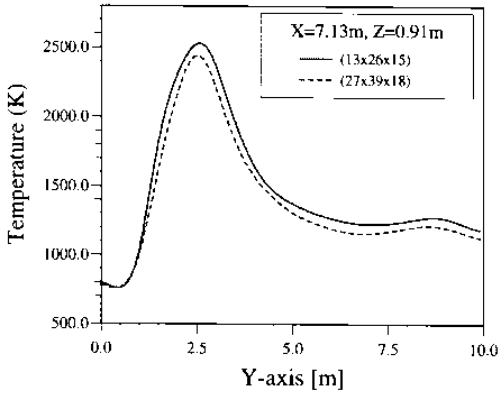

(a) Mass fractions

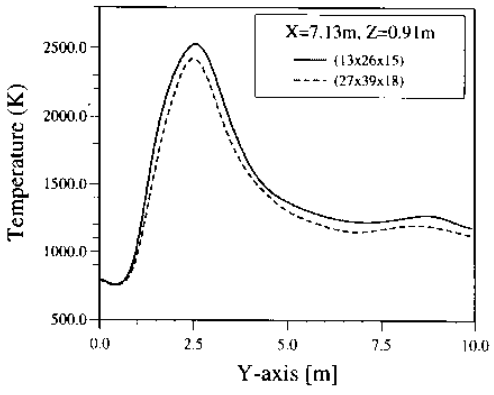

(b) Temperature

Figure 9.
Mass fraction and temperature profiles along the Y-axis at X = 7.13m, Z = 0.911m

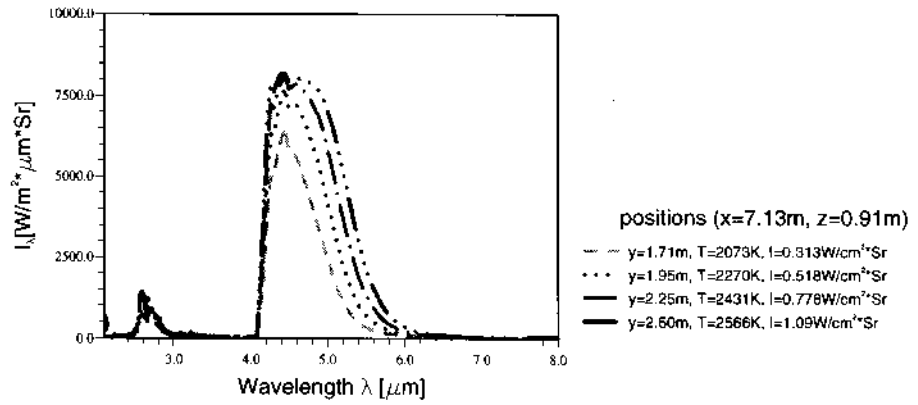

Figure 10.
Spectral intensity (Re_{inlet} = 99,876)

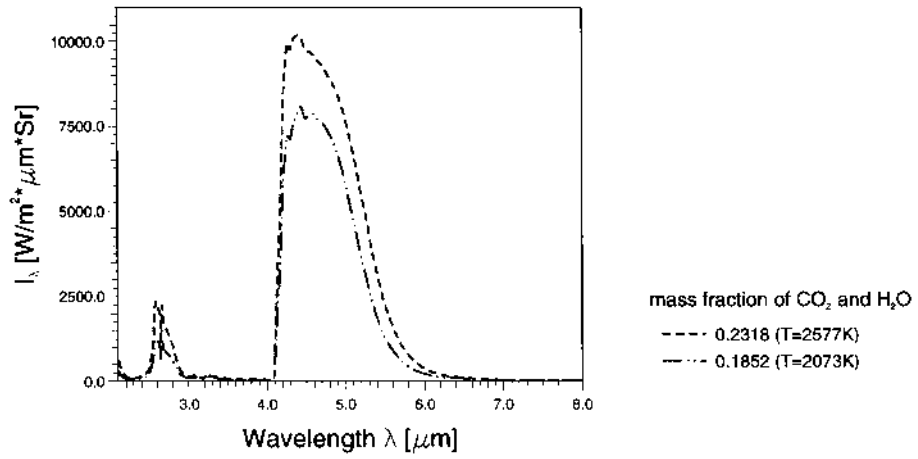

Figure 11.
Spectral intensity at an arbitrary point at different fuel inlet flow rates (X = 7.13m, Z = 0.91m)

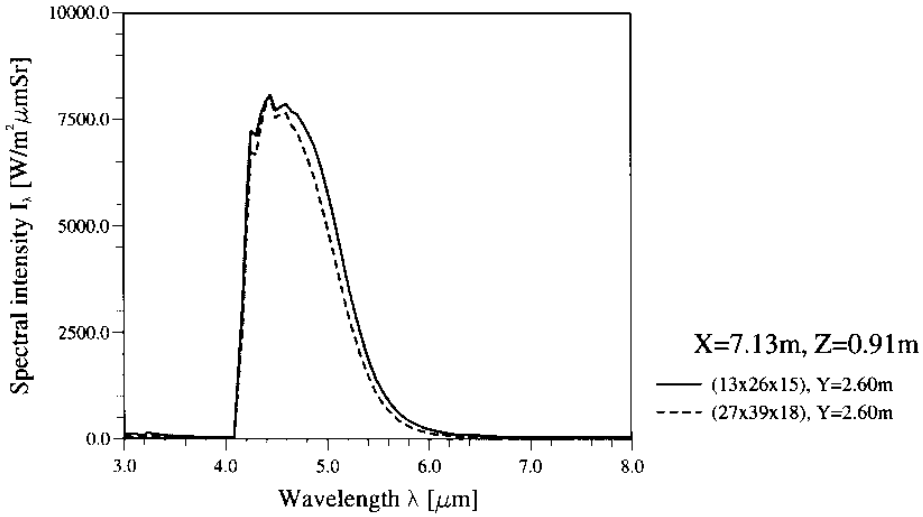

Figure 12.
Comparison of spectral intensity using two different grids (X = 7.13m, Z = 0.91m)

profiles are visible and maximum temperature and mass fraction appear at nearly the same position where the reaction has taken place. Both the temperature and mass fraction are highest in the reaction zone, and outside the flame region the temperature is nearly uniform.

Figure 10 shows how the emitted spectral intensity of the gas mixture varies with wavelength, λ, in a plane parellel to the bottom of the furnace at three different positions along the Y-direction. The spectral intensity is calculated from equation (9) for a non-homogeneous gas path.

The prediction of spectral intensity distributions around the turbulent flame are illustrated in Figure 11. The spectral intensity increases with both an increase of the mass fractions of CO_2 and H_2O, and the local temperature. This suggests that radiation intensities are significantly increased in some spectral regions owing to changes of the flow field with changes in the mass flow rate. The corresponding behaviour is caused by the rapid variation of radiation properties. Therefore, quantum mechanics ought to be employed in determining the properties of absorbing and emitting media, rather than using a wavelength independent absorption as in the gray gas model. Figure 12 shows the spectral intensity using two different grids. Predictions indicate that results are not particularly sensitive to the grid resolution.

Conclusions

A general prediction procedure for the calculation of the flow and heat transfer processes inside a three-dimensional industrial furnace has been described. The results give a clear picture of the flow pattern, temperature and turbulent kinetic energy distributions. It is suggested that simulation of the flow, heat and mass transfer in the combustion chamber can be predicted to a high level of engineering accuracy at moderately low cost by numerical procedures. We have shown in this paper the necessity for performing spectral calculations, because the flames are essentially non-luminous (non-sooting) in the infrared portion of the spectrum and a gray-medium assumption not only overestimates heat transfer but also produces inconsistent results[13]. Narrow-band statistical models provide a fundamental basis for analysing non-homogeneous radiation situations, and give the greatest flexibility for evaluating the double integral in equation (8).

References

1. Ris, De J., "Fire radiation – a review", *17th Symposium (Int.) on Combustion*, The Combustion Institute, Pittsburgh, 1979, pp. 1003-16.
2. Edwards, D.K., Glassen, L.K., Hauser, W.S. and Tuchscher, J.S., "Radiation heat transfer in nonisothermal nongray gases", *Journal of Heat Transfer*, Vol. 86C, 1967, pp. 219-29.
3. Leckner, B., "Spectral and total emissivity of water vapor and carbon dioxide", *Combustion and Flame*, Vol. 19, 1972, pp. 33-48.
4. Taine, J., "A line-by-line calculation of low-resolution radiative properties of CO_2-CO transparent nonisothermal gases mixtures up to 3000K", *Journal of Quant. Spectrosc. and Radiat. Transfer*, Vol. 30, 1983, pp. 371-9.

5. Hartmann, J.M., Levi di Leon, R. and Taine, J., "Line-by-line and narrow-band statistical model calculations for H_2O", *Journal of Quant. Spectrosc. and Radiat. Transfer*, Vol. 32 No. 2, 1984, pp. 119-27.
6. Kounalakis, M.E., Sivathanu, Y.R. and Faeth, G.M., "Infrared radiation statistics of nonluminous turbulent diffusion flames", *Journal of Heat Transfer*, Vol. 113, 1991, pp. 437-45.
7. Goody R.M., *Atmospheric Radiation*, Vol. I, Oxford, 1964.
8. Patankar, S.V., *Numerical Heat Transfer and Fluid Flow*, McGraw-Hill, New York, NY, 1980.
9. Magnussen, B.F., Hjertager, B.H., Olsen, J.G. and Bhaduri, D., "Effects of turbulent structure and local concentrations on soot formation and combustion in C_2H_2 diffusion flames", *17th Symposium (Int.) on Combustion*, The Combustion Institute, Pittsburgh, 1979, pp. 1383-93.
10. Ludwig, C.B., Malkmus, W., Reardon, J.E. and Thomas, A.J., *Handbook of Infrared Radiation from Combustion Gases*, NASA, Washington, DC, 1973.
11. Grosshandler, W.L., "A study of a model furnace burning methanol and a methanol/coal slurry", PhD dissertation, University of California, Berkeley, CA, 1977.
12. Siegel, R. and Howell, J.R., *Thermal Radiation Heat Transfer*, 3rd ed., Hemisphere Publishing Corporation, New York, NY, 1992.
13. Ahluwalia, R.K. and Im, K.H., "Spectral radiative heat-transfer in coal furnaces using a hybrid technique", *Journal of the Institute of Energy*, Vol. 67, 1994, pp. 23-9.